Automatic Segmentation of Specular Reflections for Endoscopic Images Based on Sparse and Low-Rank Decomposition

Fabiane Queiroz
Centro de Informtica
Federal University of Pernambuco - UFPE
fsq2@cin.ufpe.br

Tsang Ing Ren
Centro de Informtica
Federal University of Pernambuco - UFPE
tir@cin.ufpe.br

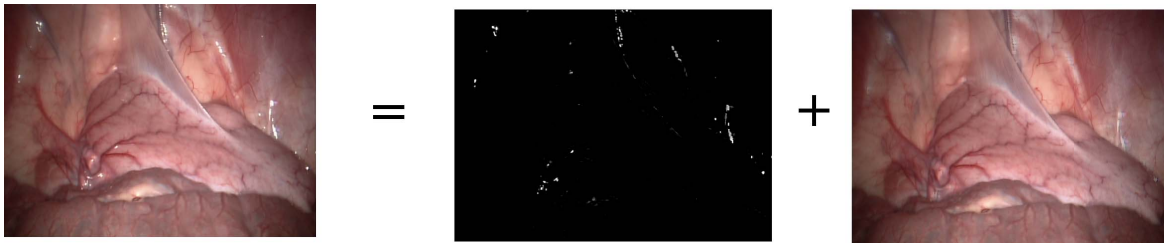

Fig. 1. From left to right: the original endoscopic image; the sparse image resulting of the decomposition - a grayscale mask containing the segmented specular reflections; the low-rank image resulting of the decomposition: image without the specular reflections.

***Abstract*—Endoscopy is a minimally invasive medical diagnostic procedure that is used to provide a realistic view of the surfaces of organs inside human body. Images taken during such procedures largely show tissues of human organs. Due to the presence of mucosa of the gastrointestinal tract or other characteristics of the human body, these surfaces usually have a glossy appearance showing specular reflections. For many image analysis algorithms, these distinct and bright visual mark can be a significant source of error. On other hand, these features can also be useful for image restoration and for the construction of 3D model of the organs. In this article, we propose a segmentation method of the specular regions based on sparse and low-rank decomposition using a robust PCA via accelerated proximal gradient algorithm. In contrast to the existing approaches, the proposed segmentation works without using colour image thresholds. Moreover, the proposed method presents more precise segmentation results represented by grayscale masks instead of binary masks.**

***Keywords*-Matrix Decomposition; robust PCA; specular reflections segmentation; medical imaging; image pocessing;**

I. Introduction

A minimally invasive medical procedure is defined as one that is carried out by a probe entering the body through the skin or through a body cavity or anatomical opening, but with the smallest damage possible to these structures. This procedure have become increasingly common in today's healthcare practice. Therefore, technological research related to this class of medical procedures is more widespread.

Endoscopy is a minimally invasive diagnostic procedure that provides the physician a realistic view of practically any part of the gastrointestinal tract or other organs inside the human body. An endoscope is a flexible tube fitted with a camera and an illumination unit at the tip. During the procedure, the performing physician can observe the endoscopic video data in real-time on a monitor. Depending on the organ that is observed there are different endoscopic procedures, for example, colonoscopy, bronchoscopy, laparoscopy and rhinoscopy. Several researches have been done in the field of endoscopic image processing including robot-assisted guidance and surgery [1], [2], [3], [4], automated documentation [5], [6] and image registration [7], [8], [9], [10].

Specular reflections usually occur on the surface of the human organs because of the endoscope frontal illumination unit. This is the cause of one of the most common image degradation [11]. Specular reflections are noticeable in images as strong highlighted regions (see, Figure 2). These marks can negatively affect the perceived image quality, and for many image analysis procedure such as segmentation (highlights may produce false regions, which becomes an obstacle for further processing), object recognition, shape form, shading etc, it can become a significant source of error [12]. On the other hand, specular reflections contains important information about the surface orientation, when the location of the light source and camera is known. The information about specular reflections may also be useful for the construction of 3D model of the organs [13] or for deconvolution methods that uses highlights information to estimate the *Point Spread Functions* (PSF's) that causes blurred images [14].

Several methods have been developed for the detection and removal of specular regions on the endoscopy images [15],

1530-1834/14 $31.00 © 2014 IEEE
DOI 10.1109/SIBGRAPI.2014.18

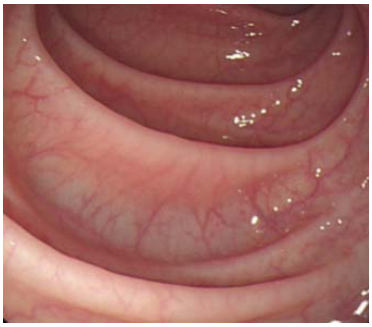

Fig. 2. Endoscopic image with specular reflections on its surface.

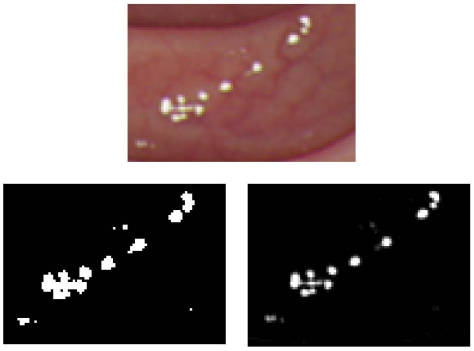

Fig. 3. Top: a close view of Figure 2. Bottom: an example of coarse (left) and precise (right) segmentation of specular reflection regions.

[16], [13], [17]. Stehle [15] selects the highest or brightest peak of the Y channel in the YUV colour space histogram as a threshold. In the work of Cao et. al. [16], the candidate regions which contain specular reflections are segmented by analysing the intensity and saturation of the pixels. In these approaches one peak value is used for thresholding the whole image, meanwhile the reflections of different intensities have different threshold values. Arnold et. al [13], uses a segmentation method of specular reflections based on nonlinear filtering and colour image thresholding. In a recent work, Karapetyan and Sarukhanyan [17] uses a sliding window of predefined size and the histogram is analysed for each window and a threshold value is selected for each window. A binary mask for the entire image that shows the candidate regions is obtained. Although the two last mentioned techniques offer better results than the ones mentioned previously, both methods still use colour thresholds.

All the methods mentioned above performs a coarse segmentation of specular reflections regions. In other words, these techniques produce binary masks that represent the map of specular reflections. In a coarse segmentation, many details of the specular reflections regions can be lost or the neighborhood of these regions can be unnecessarily segmented. The proposed segmentation performs a more precise segmentation of these regions. That is, the segmentation result is a grayscale mask that contains only specular reflections regions. The grayscale mask does not have unnecessarily neighborhood information. Figure 3 shows a close view of a coarse and precise segmentation of an endoscopic image. Here, the precise segmentation was performed using the proposed method. A precise segmentation of these specular reflections produces better results in posterior processes like inpainting [13], [17]. Moreover, many endoscopic images is affected by blur. This kind of degradation is caused by a wrong distance of the camera to the mucosa during the process of image acquisition [11], this precise segmentation of specular reflections regions can help in the process of image restoration either.

The remainder of the paper is structured as follows. Section II presents a matrix decomposition approach: the RPCA (Robust PCA) via accelerated proximal gradient algorithm [18]. Section III describes the proposed method for specular reflection segmentation of endoscopic images. Section IV shows the experimental results and comparisons with other results from the state of art. Finally, Section V concludes.

II. The Robust PCA (RPCA) via accelerated proximal gradient algorithm

Principal Component Analysis (PCA) is a statistical tool used to find patterns in data of high dimension, with applications in fields such as image processing, web data ranking, and bioinformatic data analysis. PCA offers the optimal estimate of the subspace when the data are corrupted by small Gaussian noise, but it breaks down under large corruption conditions, even if the corruption affects only a few of the observations. According to Ganesh et. al. [18], the problem of recovering a low-rank matrix from an matrix corrupted arbitrarily can be viewed as a robust version of classical PCA. Since endoscopic images are commonly affected by noise and blur [11], this work uses this robust variant of the traditional PCA to separate the input endoscopic image into its low-rank and sparse error parts.

According to Wright et.al. [19], under general conditions, one can exactly recover the low-rank matrix A from the input matrix $D = A + E$ (in this case, D is an input image of dimension $m \times n$.) with gross but sparse errors E by solving the following convex optimization problem:

$$\underset{A,E}{\text{minimize}} \quad \|A\|_* + \lambda |E|_1, \quad \text{subject to} \quad D = A + E. \tag{1}$$

where $\|\cdot\|_*$ represents the nuclear norm of a matrix (the sum of the singular values of the matrix), $|\cdot|_1$ represents the l_1 norm (the sum of the absolute values of the matrix), and λ is a positive weighting parameter. This optimization is called robust PCA (RPCA), since it enables one to correctly recover underlying low-rank structure in the data, even in the presence of huge error.

Ganesh et. al. [18] proposed a fast and scalable first-order accelerated proximal gradient algorithm to solve the expression 1. In this algorithm, they considered the following relaxed version of the RPCA optimization problem:

$$\underset{A,E}{\text{minimize}} \quad \mu\|A\|_* + \mu\lambda|E|_1 + \frac{1}{2}\|D - A - E\|_F^2 \qquad (2)$$

In this optimization problem, $f(A, B) = \frac{1}{2}\|D - A - E\|_F^2$ penalizes violations of the equality constraint, and $\mu > 0$ is a relaxation parameter. Since $f(A, B)$ is convex, smooth, and has a Lipschitz continuous gradient (with Lipschitz constant 2), the optimization problem of expression 2 is subject to efficient optimization by a group of optimization algorithms: the proximal gradient algorithms. In the work of Ganesh et. al. [18], one can see the algorithm used to solve this optimization problem in more detail. Figure 4 shows the RPCA via accelerated proximal gradient algorithm decomposition applied in a grayscale endoscopic image .

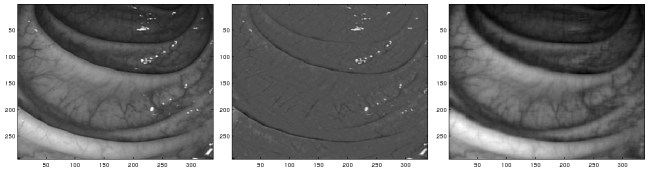

Fig. 4. The RPCA decomposition in a grayscale image. From left to right: original Image (D), the low-rank (A) of the decomposition, the error (E) of the decomposition.

III. Highlights Segmentation based on Sparse and Low-Rank Decomposition

In this work, the image decomposition approaches are used to separate the input image D into two components: the sparse one that represents a piece-wise smooth component; and the low-rank one that represents the oscillatory or texture component. The idea is that the sparse part remove the soft regions of the image while keeping the strong edges.

In general, images obtained from endoscopic procedures have a well-defined texture pattern: they have sharp specular reflections (caused by the presence of mucosa) randomly distributed over a partially homogeneous pinkish/reddish background. As can be seen in Fig. 5, this background can contains informations like veins, polyps, and other details pertinent to the gastrointestinal tract or other organs inside the human body. But these details, although visible in endoscopic images, are not as salient as the specular reflections. This strong distinction between specular reflections points and the background image is the reason for the successful use of RPCA decomposition via accelerated proximal gradient for detection of these points.

The proposed method is divided in 4 steps. Since the input D is a RGB image, in the first step, the input image D is separated in D_r, D_g and D_b: red, green, and blue colour channels respectively (see the first row of Figure 7).

In the second step, the RPCA decomposition algorithm is applied in D_r, D_g and D_b separately (Figure 4 shows this separation in the D_g channel):

$$D_r = A_r + E_r$$

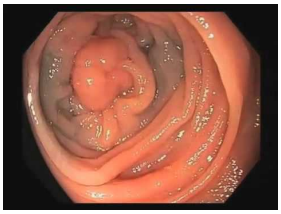

(a) Colonoscopic image showing a colonic polyp.

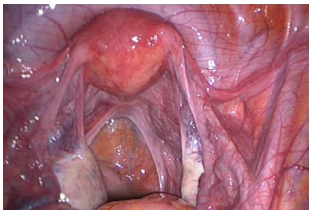

(b) Laparoscopic image.

Fig. 5. Endoscopic images.

$$D_g = A_g + E_g$$

$$D_b = A_b + E_b$$

Due the well-defined texture patterns, the error parts E_r, E_g and E_b of endoscopic images has a well-defined behaviour: they have many very high intensities values (relevant characteristic of specular reflections regions) and some very low values of pixels intensities. Figure 6 shows the histograms of the error part for each channel of the input image D, the red targets show the very low values of pixels intensities. These low values of intensities represent information of the background image, for example: less sharp edges that delimit features like veins, polypos, folds in the tissue, etc (see the second row of Figure 7). Since red target information represent not relevant information for the our purposes, we need to eliminate theses features of E_r, E_g and E_b.

In the third step, undesirable features, that is, very low values of pixels intensities of E_r, E_g and E_b are eliminated. For this, we calculated the standard deviations σ_r, σ_g and σ_b of E_r, E_g and E_b respectively, then we converted to zero all pixel values which are smaller than these standard deviations. Therefore, we generate a more sparse representations of these images: E_r^1, E_g^1 and E_b^1 (see the third rows of Figure 7).

In the fourth step, the low-rank components A_r, A_g and A_b are reformulated (see the fourth row of Figure 7):

$$A_r^1 = D_r - E_r^1$$

$$A_g^1 = D_g - E_g^1$$

$$A_b^1 = D_b + E_b^1$$

Finally, for the RGB image D, $E^1 = E_r^1 + E_g^1 + E_b^1$ represent its sparse component that contains the specular reflection (see Figure 8 - first row second column) and the final image A^1 without these specular points is represented by the merge of the colour channels A_r^1, A_g^1 and A_b^1 (see the third column of Figure 8). Inpainting methods can be applied in the final image A^1.

IV. Experiments and Results

The experiments have been done in endoscopic images from different nature: colonoscopy, bronchoscopy, laparoscopy and rhinoscopy. For all experiments, was used the λ parameter of the RPCA algorithm equals to 0.05. This value for λ was

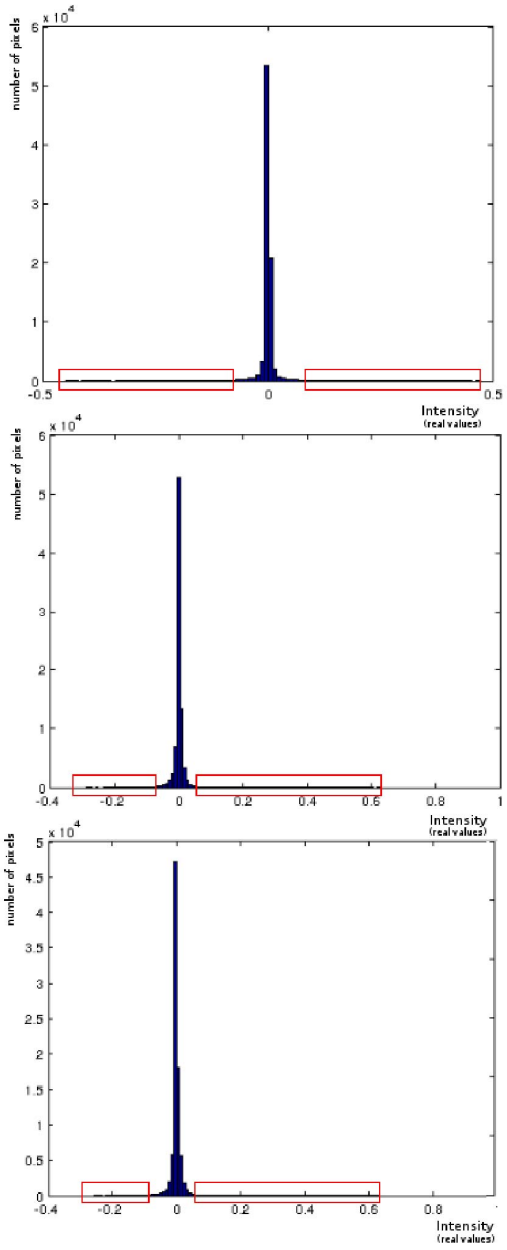

Fig. 6. From top to bottom: histograms of E_r, E_g and E_b of the RPCA decomposition.

chosen by experience. It was observed that using small values of λ parameter, very unnecessary information (pixel of very low intensities values) was segmented jointly with specular reflection regions. In other hand, increasing the value of λ has made the segmentation of the specular reflections less precise and more coarse.

Figure 9 shows two results of the application of the proposed segmentation method in two different endoscopic images. The second rows show the grayscale mask that contains the specular reflections. This mask is the sparse (E^1) part

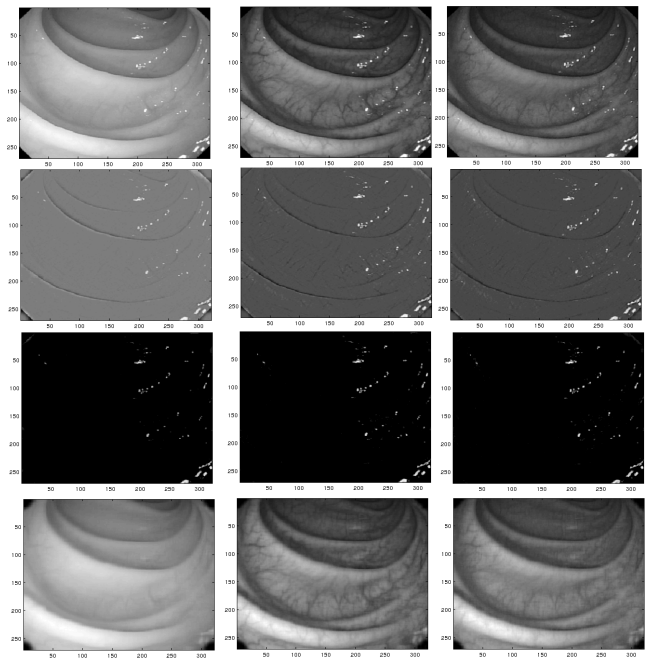

Fig. 7. From left top to right: images D_r, D_g and D_b representing the red, green and blue colour channels of an input image respectively. From top to button: original image channel, images E_r, E_g and E_b resulting from the RPCA decomposition; final sparse component; final low-rank component.

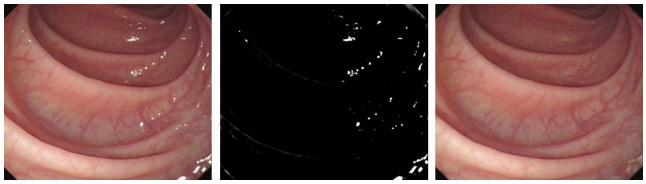

Fig. 8. From left to right: an input RGB image D; its sparse component $E^1 = E^1_r + E^1_g + E^1_b$; its low-rank component A^1.

of the decomposition. The third rows show the final image without these specular points. This image is the low-rank (A^1) part of the decomposition.

Sequential RGB image acquisition systems are frequently used in endoscopic procedures. In these systems the images that represent the red, the green and the blue colour channels are acquired at different time instances and they are merged to compose the resulting video frame. When the camera speed is high enough such that it moves significantly in the time interval between the acquisition instances of the images corresponding to two colour channels, they get misaligned in the resulting video frame. This channel misalignment generates an unnatural image, highly colourful, which degrades the video quality. The second column of Figure 9 show an image degraded by the misalignment channel. As we can see, the segmentation was successful even in this degraded image.

The proposed segmentation approach was compared with segmentation algorithms described in [13] and [17]. Both methods were assessed by their performance to classify the

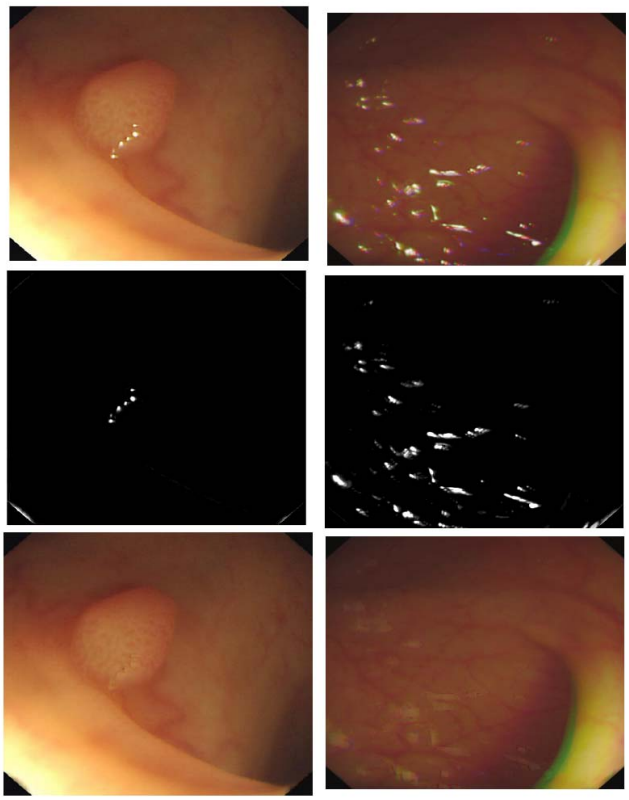

Fig. 9. Proposed method for segmentation of specular reflections using low-rank and sparse decomposition. From top to bottom: the original image D; grayscale mask containing the specular reflections - the sparse E^1 part of the decomposition; the final image without the specular reflections: the low-rank (A^1) part of the decomposition.

pixels of a given image into either specular reflection pixels or other pixels.

To create the ground truth images, a grayscale mask containing the segmented specular regions (foreground regions) was generated using the matting solution proposed by Levin et. al. [20]. After this, manually adjustments was made in this mask to remove non zero pixels that represented irrelevant informations of the input image. Figure 10 illustrates the steps for the ground truth generation.

Figure 11, 12 and 13 shows three original endoscopic images with specular reflections, the ground truth images, the segmentation proposed by the Arnold et. al [13] method and the proposed segmentation result.

The Structural SIMilarity (SSIM) index proposed by Wang et al. [21] was used to compare the similarity of the proposed results (and the results of the method proposed by Arnold al.a. [13]) with the ground truth images. The SSIM index can be viewed as a similarity measure of one of the images being compared, provided the other image that is regarded as of ground truth segmentation. The closer to 1.0000 the SSIM index value resulting from the comparison means that similarity between the ground truth images and the segmentation masks

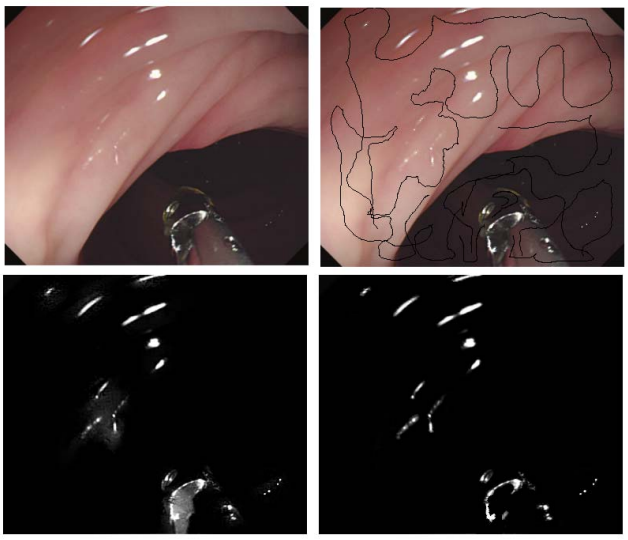

Fig. 10. From top to botton, from left to right: the original image; the image mask used as input for the matting algorithm proposed by Levin et. al. [20]- black marks indicates background regions and white marks indicates foreground regions (Specular regions); the grayscale image mask generated by the matting algorithm; final ground truth after some manual adjustments.

is better. Table I shows the SSIM index values calculated for the Arnold et.al.[13] method and the proposed method. Both results were compared with the ground truth images. As can be seen, the proposed method have the bests SSIM index values for all endoscopic images of Figures 11, 12 and 13. Based on these index values, we can affirm that the segmentation performed using the proposed method presents a more precise result because only the specular reflections are segmented. The method proposed by Arnold et. al [13] presents a coarser result where besides the specular regions, the neighborhood of these regions were also segmented. The more precise segmentation of the proposed method improve the posterior inpainting algorithm since we must inpainting smaller regions in the final low-rank image. Moreover, since the method presented by Arnold et. al [13] uses colour thresholds, some of specular reflections are not detected.

Figure 14 shows an original endoscopic images with specular reflections, the segmentation proposed by the Arnold et. al. [13], the segmentation proposed by the Karapetyan and Sarukhanyan [17] method and the proposed segmentation result. Similarly to the method presented by Arnold et. al [13], while the segmentation of the proposed method is more precise, the Karapetyan and Sarukhanyan [17] segmentation method presents a coarser result and some of specular reflections are not detected because the use of colour thresholding.

In deblurring an image, we seek to recover the original sharp image from a blurry degraded one. However, without knowledge of the blurring process, we cannot expect to recover the image perfectly. Queiroz at. al [14] propose a deblurring method of a single-image where the blur kernel of the deconvolution process is directly estimated from highlight

TABLE I
THE SSIM INDEX VALUES CALCULATED FOR THE ARNOLD ET.AL. [13] METHOD AND THE PROPOSED METHOD. BOTH RESULTS WAS COMPARED WITH THE GROUND TRUTH IMAGES.

	Arnold et. al. [13] method	Proposed Method
SSIM index value for Figure 11	0.9270	0.9999
SSIM index value for Figure 12	0.9191	0.9996
SSIM index value for Figure 13	0.9100	0.9998
SSIM index value for Figure 15: first row	0.7780	0.8352
SSIM index value for Figure 15: second row	0.8753	0.9185
SSIM index value for Figure 15: third row	0.8847	0.9582

spots or streaks with high intensity value. Therefore, creating a map of highlight, which is used as a guide to extract a single highlight from the blurred image.

Figure 16 shows that the presented segmentation method generates a good map of highlights. This map can be used in the deblurring method Queiroz at. al [14]. From this map, we extract manually one specular point. This specular point can be used as a kernel for the deconvolution process. This final result is a estimated no-blurred image.

V. CONCLUSION

In this paper, an approach for automatic segmentation of specular reflections in endoscopic images was presented. There were two main motivations for this work: 1) the nature of specular reflections and their negative affect on computer vision algorithms. 2) the use of maps of specular reflections for some image restoration algorithms. The proposed method segmented specular reflections regions with high precision generating a grayscale mask containing these regions instead binary masks. Similarity measures demonstrated the better precision of the segmentation of the proposed method compared to other recent methods from state of art.

The future work will include improvement of the segmentation algorithm as well as we will to apply this method on video sequence using data from adjacent frames.

ACKNOWLEDGMENT

The authors would like to thank this colleague and this financing institute.

REFERENCES

[1] G. N. Khan and D. F. Gillies, "Vision based navigation system for an endoscope," *Image and Vision Computing*, vol. 14, no. 10, pp. 763 – 772, 1996.

[2] S. J. Phee, W. S. Ng, I. M. Chen, F. Seow-Choen, and B. Davies, "Automation of colonoscopy. II. visual control aspects," vol. 17, no. 3, May 1998, pp. 81–88.

[3] C. K. Kwoh, G. N. Khan, and D. F. Gillies, "Automated endoscopic navigation and advisory system from medical image," in *Proc. of SPIE - Volume 3660 Medical Imaging: Physiology and Function from Multidimensional Images*, 1999.

[4] S. Voros, J.-A. Long, and P. Cinquin, "Automatic detection of instruments in laparoscopic images: A first step towards high-level command of robotic endoscopic holders." *I. J. Robotic Res.*, vol. 26, no. 11-12, pp. 1173–1190, 2007.

[5] Y. Cao, D. Li, W. Tavanapong, J. Oh, J. Wong, and P. C. de Groen, "Parsing and browsing tools for colonoscopy videos," in *Proceedings of the 12th Annual ACM International Conference on Multimedia*. New York, NY, USA: ACM, 2004, pp. 844–851.

[6] D. Iakovidis, S. Tsevas, D. Maroulis, and A. Polydorou, "Unsupervised summarisation of capsule endoscopy video," in *Intelligent Systems, 2008.*, vol. 1, Sept 2008, pp. 3–15–3–20.

[7] D. Burschka, M. Li, M. Ishii, R. H. Taylor, and G. D. Hager, "Scale-invariant registration of monocular endoscopic images to ct-scans for sinus surgery," *Medical Image Analysis*, vol. 9, no. 5, pp. 413 – 426, 2005, medical Image Computing and Computer-Assisted Intervention - {MICCAI} 2004 Medical Image Computing and Computer-Assisted Intervention.

[8] J. Liu, K. Subramanian, T. Yoo, and R. Van Uitert, "A stable optic-flow based method for tracking colonoscopy images," in *Computer Vision and Pattern Recognition Workshops, 2008. CVPRW '08. IEEE Computer Society Conference on*, June 2008, pp. 1–8.

[9] K. Mori, D. Deguchi, J.-i. Hasegawa, Y. Suenaga, J.-i. Toriwaki, H. Takabatake, and H. Natori, "A method for tracking the camera motion of real endoscope by epipolar geometry analysis and virtual endoscopy system," in *Medical Image Computing and Computer-Assisted Intervention ? MICCAI 2001*, ser. Lecture Notes in Computer Science, W. Niessen and M. Viergever, Eds. Springer Berlin Heidelberg, 2001, vol. 2208, pp. 1–8.

[10] C. Wengert, P. Cattin, J. Duff, C. Baur, and G. Szkely, "Markerless endoscopic registration and referencing," in *Medical Image Computing and Computer-Assisted Intervention MICCAI 2006*, ser. Lecture Notes in Computer Science, R. Larsen, M. Nielsen, and J. Sporring, Eds. Springer Berlin Heidelberg, 2006, vol. 4190, pp. 816–823.

[11] S. Hegenbart, A. Uhl, and A. Vecsei, "Impact of endoscopic image degradations on LBP based features using one-class svm for classification of celiac disease," in *Image and Signal Processing and Analysis (ISPA)*, Sept 2011, pp. 715–720.

[12] F. Vogt, D. Paulus, B. Heigl, C. Vogelgsang, H. Niemann, G. Greiner, and C. Schick, "Making the invisible visible: Highlight substitution by color light fields," 2002, pp. 352 – 357.

[13] M. Arnold, A. Ghosh, S. Ameling, and G. Lacey, "Automatic segmentation and inpainting of specular highlights for endoscopic imaging," *J. Image Video Process.*, vol. 2010, pp. 9:1–9:12, Jan. 2010.

[14] F. Queiroz, T. I. Ren, L. Shapira, and R. Banner, "Image deblurring using maps of highlights." in *ICASSP*. IEEE, 2013, pp. 1608–1611.

[15] T. Stehle, "Removal of specular reflections in endoscopic images," *Acta Polytechnica: Journal of Advanced Engineering*, vol. 46, no. 4, pp. 32–36, 2006.

[16] Y. Cao, D. Liu, W. Tavanapong, J. Wong, J. Oh, and P. de Groen, "Computer-aided detection of diagnostic and therapeutic operations in colonoscopy videos," *Biomedical Engineering, IEEE Transactions on*, vol. 54, no. 7, pp. 1268–1279, July 2007.

[17] G. Karapetyan and H. Sarukhanyan, "Automatic detection and concealment of specular reflections for endoscopic images," in *Computer Science and Information Technologies (CSIT), 2013*, Sept 2013, pp. 1–8.

[18] A. Ganesh, Z. Lin, J. Wright, L. Wu, M. Chen, and Y. Ma, "Fast algorithms for recovering a corrupted low-rank matrix," in *Computational Advances in Multi-Sensor Adaptive Processing (CAMSAP), 2009 3rd IEEE International Workshop on*, Dec 2009, pp. 213–216.

[19] J. Wright, A. Ganesh, S. Rao, Y. Peng, and Y. Ma, "Robust principal component analysis: Exact recovery of corrupted low-rank matrices via convex optimization," in *NIPS*, 2009, pp. 2080–2088.

[20] A. Levin, D. Lischinski, and Y. Weiss, "A closed-form solution to natural image matting," *Pattern Analysis and Machine Intelligence, IEEE Transactions on*, vol. 30, no. 2, pp. 228–242, Feb 2008.

[21] Z. Wang, A. Bovik, H. Sheikh, and E. Simoncelli, "Image quality assessment: from error visibility to structural similarity," *Image Processing, IEEE Transactions on*, vol. 13, no. 4, pp. 600–612, April 2004.

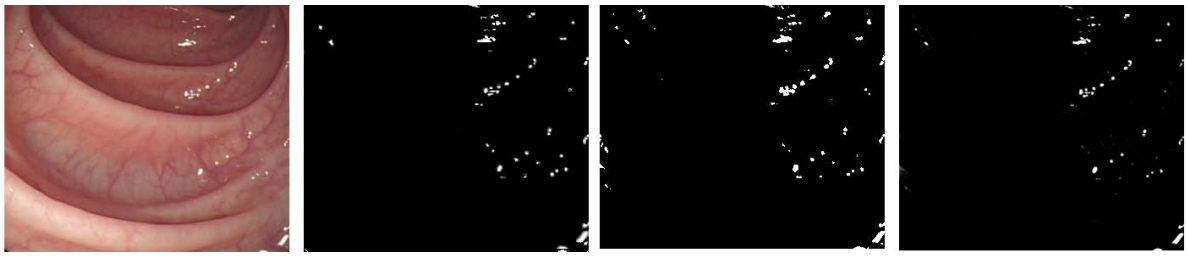

Fig. 11. From left to right: the original endoscopic image; the ground truth image mask of specular reflections; the mask of specular reflections generated by the Arnold et. al [13] method; the mask of specular reflections generated by the proposed method - this mask is the sparse part (E^1) of the sparse and low-rank decomposition applied in the original image.

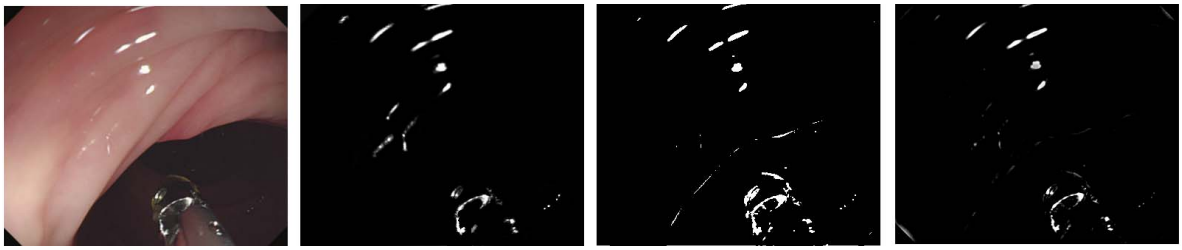

Fig. 12. From left to right: the original endoscopic image; the ground truth image mask of specular reflections; the mask of specular reflections generated by the Arnold et. al [13] method; the mask of specular reflections generated by the proposed method - this mask is the sparse part (E^1) of the sparse and low-rank decomposition applied in the original image.

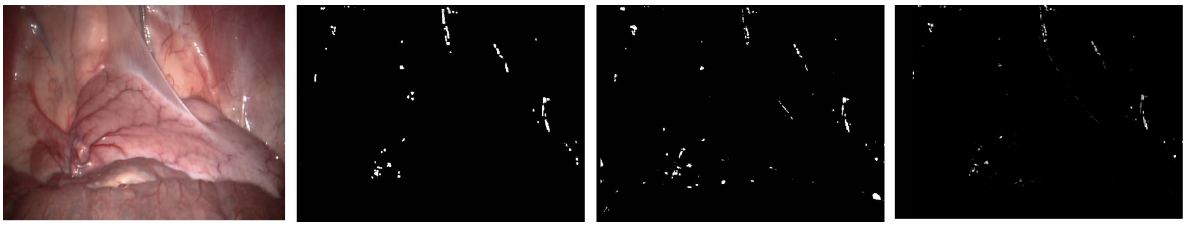

Fig. 13. From left to right: the original endoscopic image; the ground truth image mask of specular reflections; the mask of specular reflections generated by the Arnold et. al [13] method; the mask of specular reflections generated by the proposed method - this mask is the sparse part (E^1) of the sparse and low-rank decomposition applied in the original image.

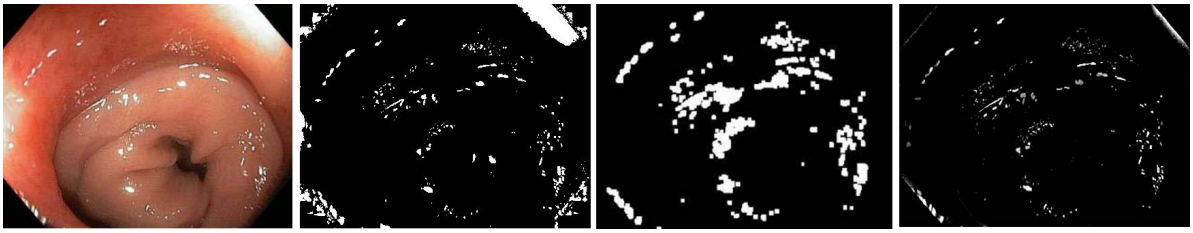

Fig. 14. From left to right: the original endoscopic image; the segmentation proposed by the Arnold et. al. [13]; the segmentation of specular reflection by the Karapetyan and Sarukhanyan [17] method; the proposed segmentation method using sparse part (E^1) of the sparse and low-rank decomposition.

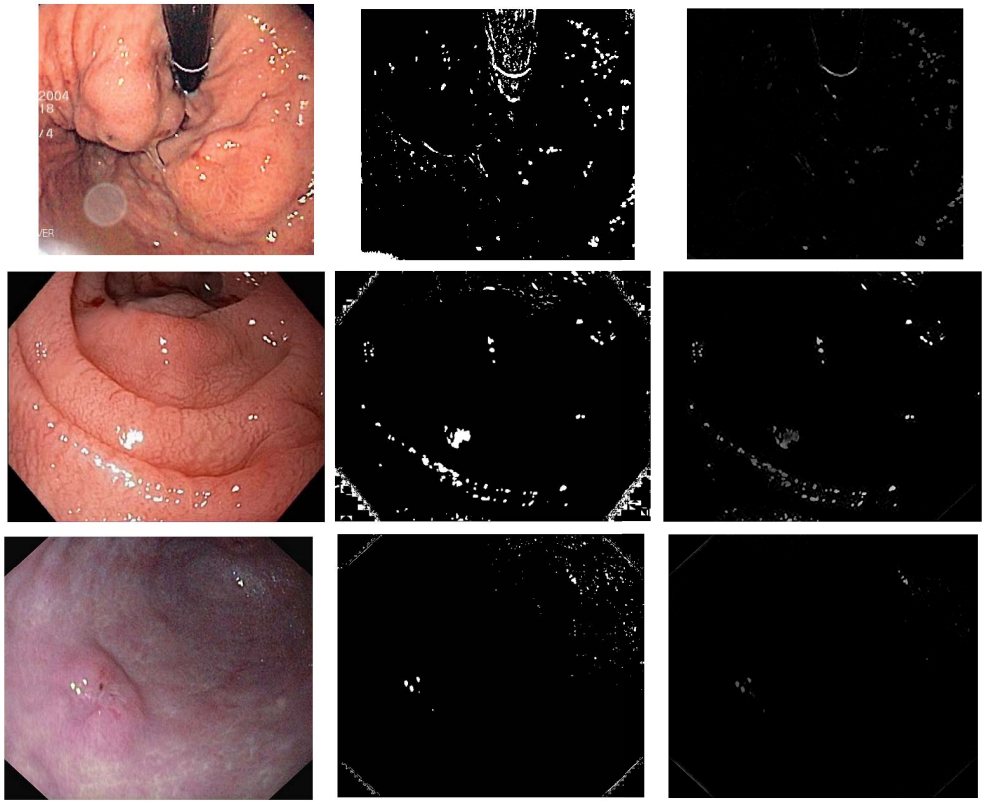

Fig. 15. From left to right: the original endoscopic image; the mask of specular reflections generated by the Arnold et. al [13] method; the mask of specular reflections generated by the proposed method - this mask is the sparse part (E^1) of the sparse and low-rank decomposition applied in the original image.

Fig. 16. From left to right: original input image; the input image degraded by motion blur;the segmented specular reflections in the degraded image using sparse and low-rank decomposition; deblurred image and kernel of convolution using the deblur method proposed by Queiroz et. al [14].